Supporting Information for "Dynamics of a Solidifying Icy Satellite Shell"

J. J. Buffo[1], C. R. Meyer[1], and J. R. G. Parkinson[2]

[1]Thayer School of Engineering, Dartmouth College, Hanover, NH 03755, USA

[2]Atmospheric, Oceanic and Planetary Physics, Department of Physics, Clarendon Laboratory, University of Oxford, Parks Road, Oxford OX1 3PU, UK

Contents of this file

1. Text S1 to S4
2. Figures S1 to S6
3. Movies S1 to S2

Introduction

Below we include four supplementary sections which aim to bolster the conclusions of the main manuscript. Section S1 provides an independent validation of the two-dimensional multiphase reactive transport model (SOFTBALL (Parkinson et al., 2020)) utilized throughout the work via simulations of sea ice growth and explores the impact of variable permeability on the efficiency of impurity entrainment. Section S2 supports the implementation of a linear conductive profile approximation for estimating the ice-ocean interface thermal gradient by comparing simulated and approximated ice shell thermal profiles. Section S3 builds on and supports the work of Section 3.3 of the main manuscript by comparing the brine channel spacing produced under Europan conditions to those predicted by contemporary models simulating terrestrial ice-ocean/brine environments (Wells

et al., 2011; Parkinson, 2019). Section S4 discusses potential limitations of the single domain Darcy velocity approach for investigating the geometry and longevity of brinicles.

Text S1 - Model Validation

To independently validate the two-dimensional reactive transport model of Parkinson et al. (2020) we simulated the physicochemical evolution of sea ice under simplified polar conditions. Model runs were initiated by assuming the domain was entirely filled with seawater (35 ppt) just above it's melting temperature (-1.68C), subject to an undercooled atmosphere above (-23.15C) and an ambient ocean below (-1.68C). To ensure the model produces consistent results across a range of spatial scales (important for our upscaling to the Europa environment), we carried out four different runs at varying resolutions, the results of which can be seen in Figure S1. While it is clear that the detailed structure of brine channels within the ice layer are less well resolved when a coarser resolution is employed, the overall bulk salinity profile of the ice is maintained across all resolutions. This can be seen by horizontally averaging the two-dimensional bulk concentration profiles of Figure S1. The results of such an averaging can be seen in Figure S2, which depicts bulk salinity profiles for all four simulated resolutions of Figure S1. There exists only minor variations in bulk salinity, primarily near the ice-ocean interface, where the coarsest resolution simulation struggles to resolve details of the phase change interface between 0.75-0.85 m. Additionally, the simulated bulk salinity profiles qualitatively and quantitatively match empirical measurements of both natural and laboratory grown sea ice (e.g. (Eicken, 1992; Nakawo & Sinha, 1981; Notz et al., 2005)), exhibiting a characteristic 'c-shape' salinity profile with amplified salinities near both the upper ice-atmosphere interface and the basal ice-ocean interface as well as bulk salinity values well within the observational range (Eicken, 1992; Nakawo & Sinha, 1981; Notz et al., 2005). The ability of the model to reproduce bulk salinity profiles of sea ice provides an additional and

independent validation of the model, expanding upon the existing literature (Parkinson, 2019; Parkinson et al., 2020; Wells et al., 2019), and lending confidence to the model's application to planetary ice-ocean systems.

An important, yet under constrained, component of nearly all multiphase ice models is the implementation of a permeability-porosity relationship (e.g. (Golden et al., 2007; Katz & Worster, 2008; Buffo et al., 2020; Parkinson et al., 2020)). This relationship governs the ability of fluid to flow throughout the system and aims to broadly capture the fine-scale microstructural properties of the complex porous ice matrix. This is a common challenge in porous media studies and a range of permeability-porosity relationships exist (Bear, 2013). Our selection of a Kozeny-Carman permeability-porosity relationship for our Hele-Shaw cell simulations is consistent with previous studies of unidirectional ice-brine solidification investigations (Katz & Worster, 2008; Parkinson et al., 2020; Wells et al., 2019). Nevertheless, this relationship (Equation 7 of the main text) relies on the selection of a permeability factor, K_0. This is akin to the reference permeabilities in the power law permeability-porosity relationships of other multiphase ice-brine system studies (e.g. (Hammond et al., 2018; Golden et al., 2007)). Regardless, the selection of this parameter will impact the permeability, and thus fluid transport, of the system and should reproduce empirical observations of ocean-derived ices. To demonstrate the importance of the permeability factor (K_0) we simulated the physicochemical evolution of sea ice (as described above) using a range of permeability factors and compared their resulting bulk salinity profiles. The results of these simulations can be seen in Figure S3. In varying the permeability factor by a factor of 20 bulk salinity in regions of the ice varied by as much as 30%. Such variations can have drastic effects on the properties of the resultant ice, and highlights the need to further constrain our understanding of ocean-derived ice permeability via both experimental and numerical techniques. Our selected value of

K_0 used throughout the study $K_0 = 2 \times 10^{-9}\ m^2$ produces bulk salinity profiles consistent with observations of natural and laboratory grown sea ice (Eicken, 1992; Nakawo & Sinha, 1981; Notz et al., 2005). Furthermore, the Hele-Shaw cell limited Kozeny-Carman relationship employed in our work is consistent with empirically derived power law permeability-porosity relationships for sea ice (Golden et al., 2007). Figure S4 shows a comparison of the power law permeability-porosity relationship derived empirically by Golden et al. (2007), the power law relationship employed in the modeling investigation of Buffo et al. (2020), the Kozeny-Carman permeability-porosity relationship employed in the manuscript (without Hele-Shaw cell limitation), and the same Kozeny-Carman permeability-porosity relationship when it is employed in a Hele-Shaw cell, limiting the permeability of the free fluid to a finite value. While there are slight variations in the predicted permeability values, for porosities relevant to the interior of the mushy layer ($\phi < 0.8$) predicted permeabilities are within two orders of magnitude.

Text S2 - Ice Shell Thermal Profile

To demonstrate the validity of implementing the simple linear conduction approximation for the ice-ocean interface thermal gradient (Equation 8 of the main text), we compare the thermal profile during a selected simulation to that predicted by the linear conduction approximation:

$$T(z) = T_s + \frac{T_{oc} - T_s}{H_{shell}} z \tag{1}$$

where z is depth beneath the surface, T_{oc} is ocean temperature, T_s is the surface temperature, and H_{shell} is the thickness of the ice shell. The results of this comparison can be seen in Figure S5. The profiles vary only slightly, with true temperatures being slightly higher throughout the majority of the shell. This is an expected result as the ice-ocean interface mushy layer will buffer heat loss to the cold upper surface due to the lower ther-

mal conductivity of brine compared to ice. Such variations in ice shell thermal profiles have previously been shown to have a negligible affect on interface dynamics and ice shell physicochemical characteristics (Buffo et al., 2020).

Text S3 - Brine Channel Spacing

The distribution of brine channels in the mushy layer plays a fundamental role in the desalination and structure of the ice-ocean interface, and thus the physicochemical properties of ocean-derived ices. Channel spacing is a dynamic property and depends on a number of environmental pressures which control convective motion in the porous region near the ice-ocean phase boundary. Brine channel spacing in saltwater systems has previously been investigated, both experimentally (Wakatsuchi & Saito, 1985; Tison & Verbeke, 2001) and theoretically (Wells et al., 2011; Parkinson, 2019). Wells et al. (2011) and Parkinson (2019) demonstrate that the non-dimensional brine channel aspect ratio, defined as:

$$a_s = \frac{L}{2h} \tag{2}$$

where L is the horizontal distance between brine channels and h is the thickness of the ice-ocean interface mushy layer, is strongly controlled by the mush Rayleigh number (Wells et al., 2011; Parkinson, 2019):

$$Ra_{ML} = \frac{K_0 \rho_{br} g \beta \Delta C h}{\kappa_{br} \eta} \tag{3}$$

where K_0 is a characteristic permeability, ρ_{br} is the density of the underlying ocean/brine, g is gravity, β is the solutal contraction coefficient, ΔC is the difference in salinity between the eutectic concentration and the underlying fluid, h is mushy layer thickness, κ_{br} is the thermal diffusivity of the underlying fluid, and η is dynamic fluid viscosity.

To investigate the relationship between ice-ocean interface environment and brine channel spacing, in both planetary and terrestrial systems, we measured brine channel aspect ratios for seven simulations (ice shell depths ranging from 10 m to 1000 m) under Europan conditions and compare our results to those of Wells et al. (2011) and Parkinson (2019) (Figure S6). Additionally, we measured brine channel aspect ratios during a simulation of sea ice to ensure our results agree with those of Parkinson (2019) who simulate the top-down solidification of sea ice under a range of thermal forcing and during a simulation where a concentration ratio $\mathcal{C}$=1 is implemented to bridge the existing gap between the concentration ratios investigated by Wells et al. (2011) ($\mathcal{C}$=2,5,10,15) and those utilized in Parkinson (2019) and the current work ($\mathcal{C}$=0.18). Following Wells et al. (2011), the concentration ratio is defined as:

$$\mathcal{C} = \frac{C_0 - C_s}{C_e - C_0} \tag{4}$$

where C_0 is the salinity of the underlying fluid, C_s is the salinity of ice (here taken to be zero), and C_e is the eutectic concentration.

Our simulation results, as well as the results of Wells et al. (2011) and Parkinson (2019), show a general trend of decreasing brine channel aspect ratio with increasing mush Rayleigh number, approaching a steady state value for $Ra_{ML} >> Ra_c$, as reported by Wells et al. (2011), where Ra_c is the critical Rayleigh number where mushy layer convection initiates. This suggests that after onset of convection in the mushy layer the rate of mushy layer thickening (increasing h) outpaces the collapse/merging of brine channels (a phenomenon well documented in the literature by both experimental and modeling studies, which leads to increasing L), until a steady state aspect ratio is achieved. The primary environmental factor affecting the value of the steady state aspect ratio is the concentration ratio, for while simulations of sea ice and Europan ice had substantially

different environmental forcing (gravity, characteristic permeability) their steady state aspect ratios vary minimally when compared to the difference in steady state aspect ratios of simulations with variable concentration ratios. An additional control on brine channel spacing is the finite width of our simulation domain, which necessarily quantizes the number of brine channels. We have taken care to select domain widths which facilitate a large number of brine channels whenever possible to reduce the impact of this numerical limitation. Another interesting feature of the simulations presented in Figure S6 is the existence of convective modes; apparent in all simulations except those of Wells et al. (2011), due to their method of selecting L such that it maximized solute flux from the mushy layer (Wells et al., 2012) and observing the evolution of h, as jumps between well defined groupings that are well represented by the inverse fits of Figure S6 (additionally, transition between convective modes can be seen in Supplementary Movie S1 and S2 as brine channels collapse and reform). This alternation between quasi-stable convective modes in a confined porous media is a well documented natural phenomenon (e.g. (Karani & Huber, 2017)) which we believe is amplified by the finite resolution of the simulations. That is, as the resolution is coarsened, as is needed to simulate thicker mushy layers deep within the ice shell of Europa, the lower modes (associated with smaller aspect ratios) are likely not explicitly resolved by the simulation. This does not affect the accuracy of the physicochemical results of the model, however, as it was shown in Section S1 that bulk salinity profiles remain constant regardless of whether discrete brine channels are resolved (e.g. Figures S1 S2).

Due to the rapid rate at which ice-ocean systems exceed their critical Rayleigh numbers (e.g. the presence of brine channels in thin sea ice (Wettlaufer et al., 1997; Cox & Weeks, 1974)) we conclude that the thick ice shells of icy worlds such as Europa should have ice-ocean interfaces characterized by brine channel aspect ratios near their steady

state limit. This suggests progressively widening channel spacing as the ice shell thickens that will scale with mushy layer thickness. Given the results of Section 3.2 of the main manuscript (that mushy layer thickness can be well approximated as a linear function of ice shell thickness, linear relationship coefficient=0.0539), and noting that the steady state brine channel aspect ratio is 0.08 (Blue lines of Figure S6), Europan ice shells of thickness 1 km, 10 km, and 30 km would have expected brine channel spacing of 8.62 m, 86.2 m, and 259 m, respectively. Constraining channel spacing is important in understanding the desalination and heterogeneity of the lower ice shell, which may have substantial implications for the geophysical processes and habitability of ice-ocean worlds, as outlined in the main manuscript.

Text S4 - A Note on Simulated Brinicle Geometry

It is important to note that the geometry of the brinicles simulated in Section 3.3 may be impacted by the Darcy approximation implemented in the SOFTBALL code. The Darcy technique is employed to simplify the ice-ocean system and involves simulating the entire domain (liquid and solid) as a porous media (rather than solving Darcy's law in the porous region and the Navier-Stokes equation in the fluid). This is a widely used method and its accuracy hinges on the large amplification of permeability in the fluid region (compared to the porous region). A large, but finite, permeability means flow is faster in the fluid than in the porous region (ensuring accurate evolution of the multiphase layer), while still being computationally tractable and avoiding a difficult boundary value problem. The reduction of flow speed in the free fluid from its true value (permeability $\neq$ infinity), however, means that diffusive processes are likely overly expressed in the fluid region. This could lead to amplified spacing between brinicle walls beneath downwelling high salinity regions (e.g. Figure 6). In the real system downwelling plumes will not be subject to a finite permeability and are likely to be more jet-like, reducing dissipative

flow near the interface and potentially supporting more stable, longer-lived ice structures than suggested in Section 3.3 (See Wells et al. (2019)). We therefore suggest our results be taken as a lower limit for the longevity of brinicle structures at Europa's ice-ocean interface.

Movie S1.

Nondimensional bulk salinity evolution under Europan conditions. (Domain: 20m x 20m (512 x 512 grid), Resolution: 3.9cm)

Movie S2.

Porosity evolution under Europan conditions. (Domain: 20m x 20m (512 x 512 grid), Resolution: 3.9cm)

References

Bear, J. (2013). *Dynamics of fluids in porous media* [Book]. Courier Corporation.

Buffo, J. J., Schmidt, B. E., Huber, C., & Walker, C. C. (2020). Entrainment and dynamics of ocean-derived impurities within europa's ice shell [Journal Article]. *JGR: Planets*.

Cox, G. F. N., & Weeks, W. F. (1974). Salinity variations in sea ice [Journal Article]. *Journal of Glaciology*, *13*(67), 109-120.

Eicken, H. (1992). Salinity profiles of antarctic sea ice: field data and model results [Journal Article]. *Journal of Geophysical Research: Oceans*, *97*(C10), 15545-15557.

Golden, K. M., Eicken, H., Heaton, A. L., Miner, J., Pringle, D. J., & Zhu, J. (2007). Thermal evolution of permeability and microstructure in sea ice [Journal Article]. *Geophysical Research Letters*, *34*(16).

Hammond, N. P., Parmenteir, E., & Barr, A. C. (2018). Compaction and melt transport in ammonia-rich ice shells: Implications for the evolution of triton [Journal Article]. *Journal of Geophysical Research: Planets*, *123*(12), 3105-3118.

Karani, H., & Huber, C. (2017). Transitional behaviour of convective patterns in free convection in porous media [Journal Article]. *Journal of Fluid Mechanics*, *818*.

Katz, R. F., & Worster, M. G. (2008). Simulation of directional solidification, thermochemical convection, and chimney formation in a hele-shaw cell [Journal Article]. *Journal of Computational Physics*, *227*(23), 9823-9840.

Nakawo, M., & Sinha, N. K. (1981). Growth rate and salinity profile of first-year sea ice in the high arctic [Journal Article]. *Journal of Glaciology*, *27*(96), 315-330.

Notz, D., Wettlaufer, J. S., & Worster, M. G. (2005). A non-destructive method for measuring the salinity and solid fraction of growing sea ice in situ [Journal Article]. *Journal of Glaciology*, *51*(172), 159-166.

Parkinson, J. R. G. (2019). *Nonlinear convection in sea ice and other mushy layers* (Thesis). University of Oxford.

Parkinson, J. R. G., Martin, D. F., Wells, A. J., & Katz, R. F. (2020). Modelling binary alloy solidification with adaptive mesh refinement [Journal Article]. *Journal of Computational Physics: X*, *5*, 100043.

Tison, J.-L., & Verbeke, V. (2001). Chlorinity/salinity distribution patterns in experimental granular sea ice [Journal Article]. *Annals of Glaciology*, *33*, 13-20.

Wakatsuchi, M., & Saito, T. (1985). On brine drainage channels of young sea ice [Journal Article]. *Annals of glaciology*, *6*, 200-202.

Wells, A. J., Hitchen, J. R., & Parkinson, J. R. (2019). Mushy-layer growth and convection, with application to sea ice [Journal Article]. *Philosophical Transactions of the Royal Society A*, *377*(2146), 20180165.

Wells, A. J., Wettlaufer, J., & Orszag, S. (2011). Brine fluxes from growing sea ice [Journal Article]. *Geophysical Research Letters*, *38*(4).

Wells, A. J., Wettlaufer, J. S., & Orszag, S. A. (2012). Nonlinear mushy-layer convection

with chimneys: stability and optimal solute fluxes [Journal Article]. *arXiv preprint arXiv:1205.0964*.

Wettlaufer, J., Worster, M. G., & Huppert, H. E. (1997). Natural convection during solidification of an alloy from above with application to the evolution of sea ice [Journal Article]. *Journal of fluid mechanics*, *344*, 291-316.

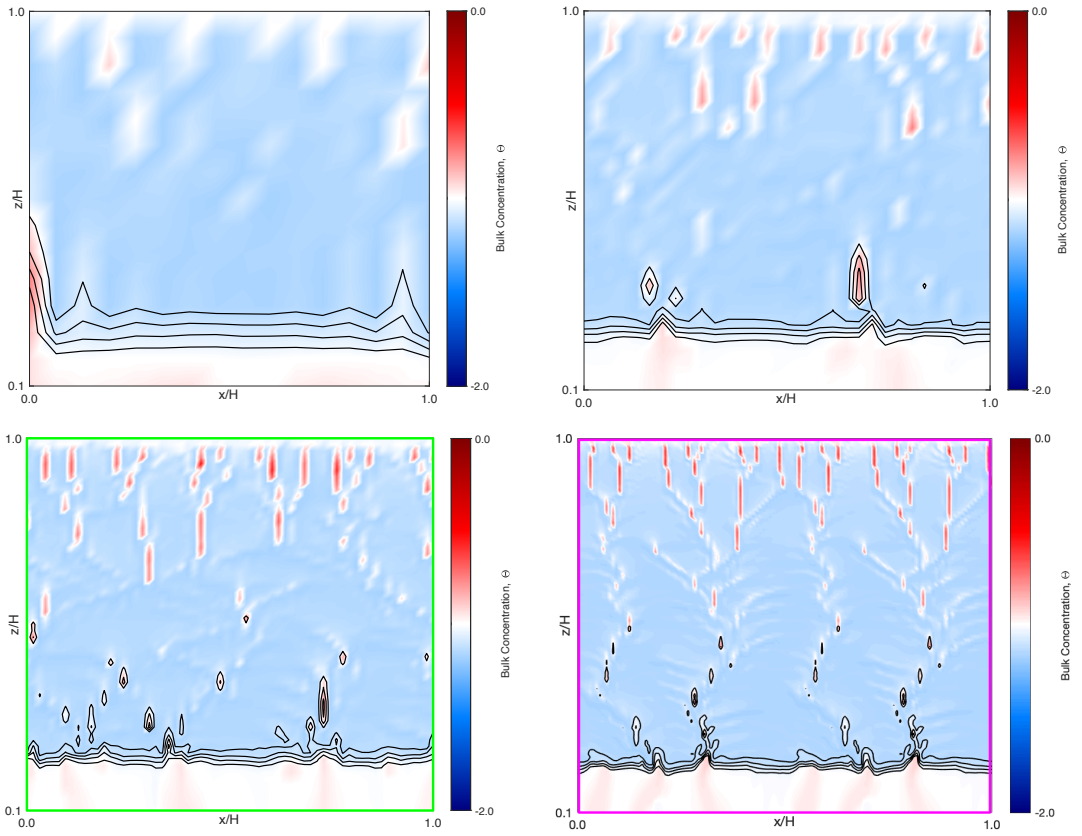

Figure S1. The effects of variable resolution. **Top Left)** 16x16 starting grid, no Adaptive Mesh Refinement (AMR) (6.25 cm resolution). **Top Right)** 32x32 starting grid, no AMR (3.13 cm resolution). **Bottom Left)** 32x32 starting grid, 1 level AMR (1.56 cm resolution). **Bottom Right)** 32x32 starting grid, 2 level AMR (0.78 cm resolution).

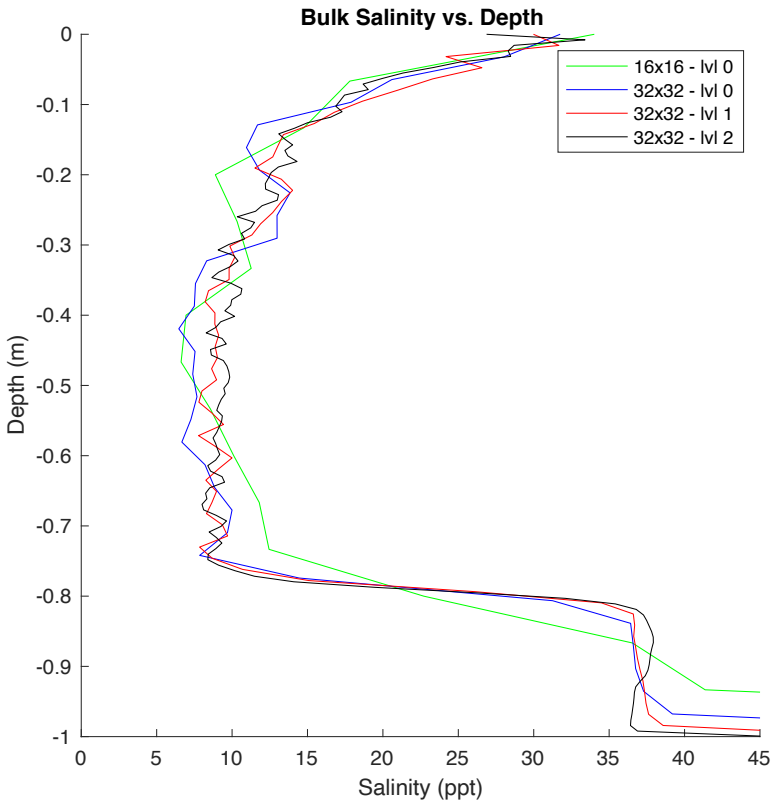

Figure S2. Horizontally averaged bulk salinity profiles. Using the results of Figure S1, bulk salinity is horizontally averaged and compared. Profiles have characteristic 'c-shape' of first year sea ice, with appropriate bulk salinity values, and are in good agreement across all resolutions.

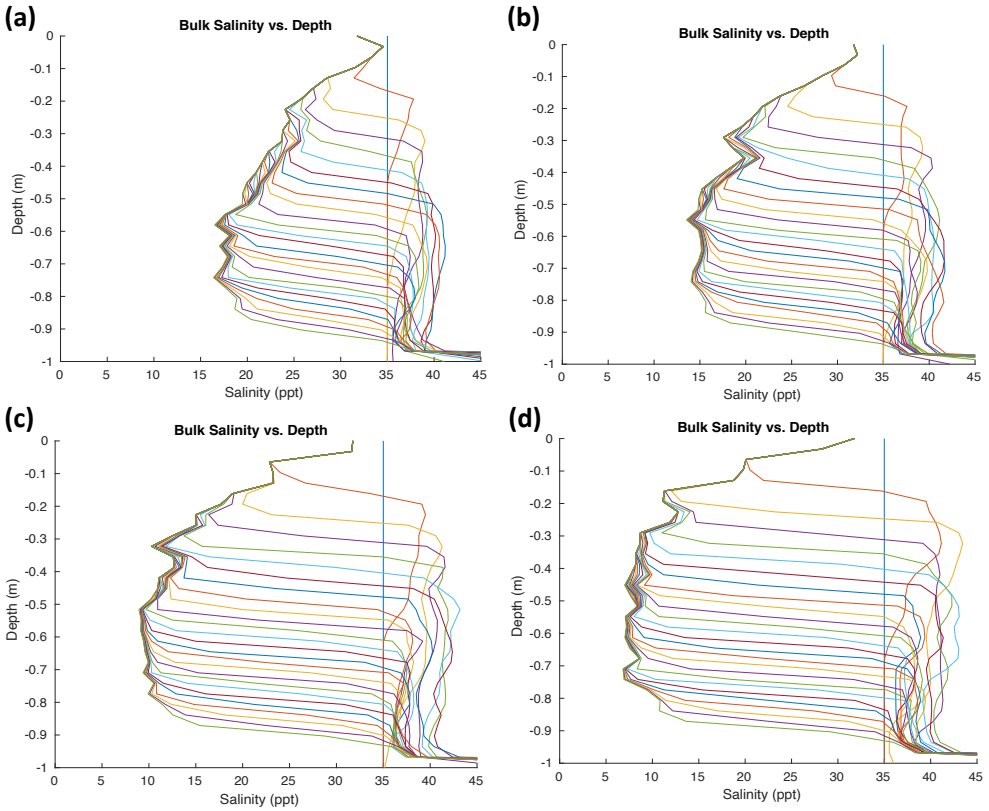

Figure S3. The effects of variable permeability factors on sea ice bulk salinity. Horizontally averaged bulk salinity profiles of sea ice generated using identical conditions less the permeability factor, K_0. **a)** $K_0 = 1e^{-10}$. **b)** $K_0 = 2e^{-10}$. **c)** $K_0 = 8e^{-10}$. **d)** $K_0 = 2e^{-9}$. In all plots colors represent progressive temporal snapshots during the simulation (as the ice thickens).

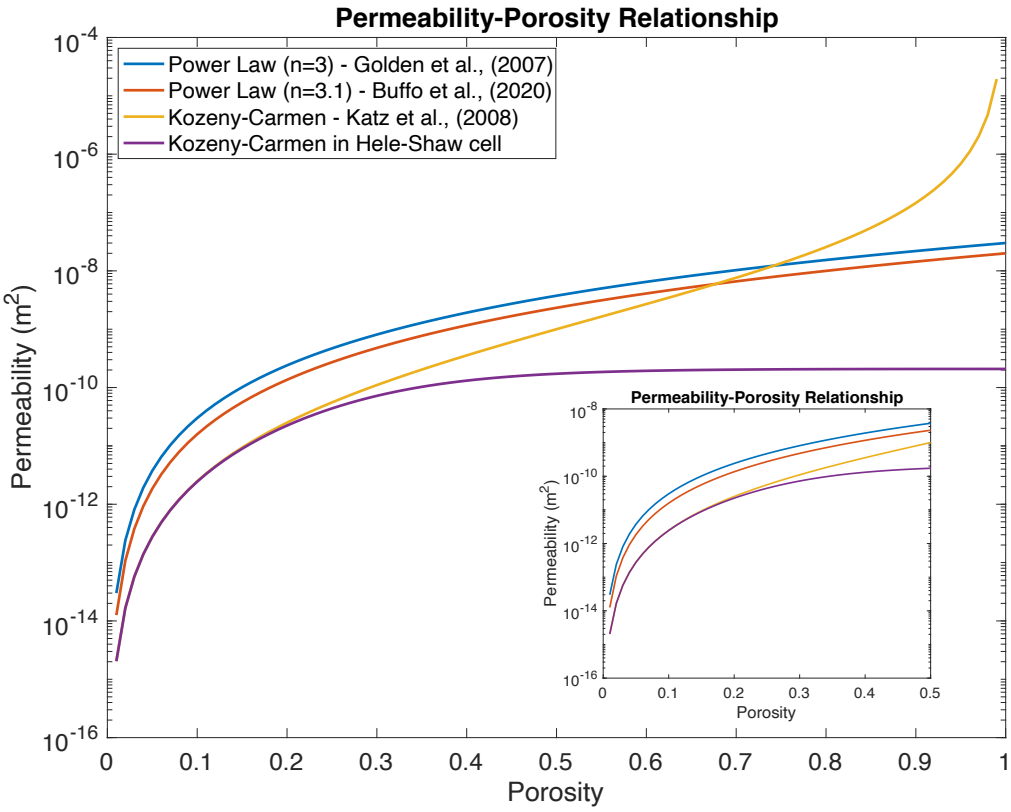

Figure S4. A comparison of common permeability-porosity relationships. The modified Kozeny-Carmen relationship of Parkinson et al. (2020) (purple line), employed here, is comparable to the Kozeny-Carmen relationship of Katz and Worster (2008) as well as the power law relationships of Golden et al. (2007) and Buffo et al. (2020). The Hele-Shaw cell modifications place a finite limit on the permeability of the underlying fluid ($\phi \to 1$).

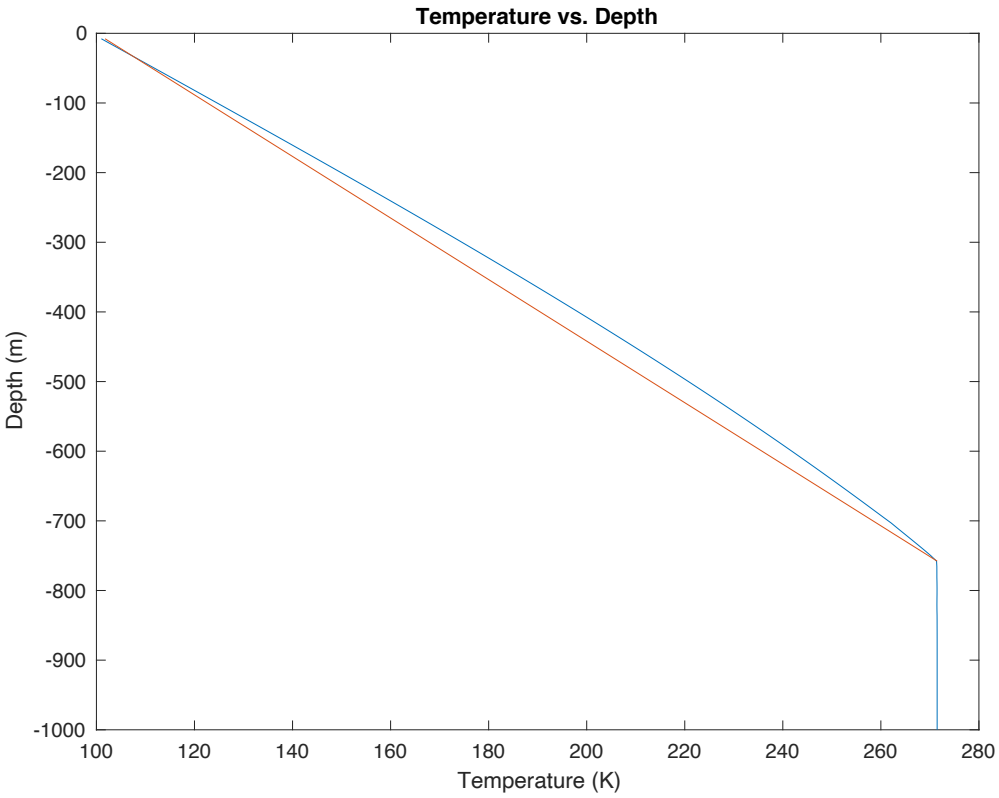

Figure S5. Thermal profiles in an ice shell. The blue curve is the horizontally averaged temperature profile extracted from a top-down solidification simulation under Europa conditions. The ice-ocean interface occurs at ∼758 m below the surface. The red curve is the linear conduction approximation given by Equation S1.

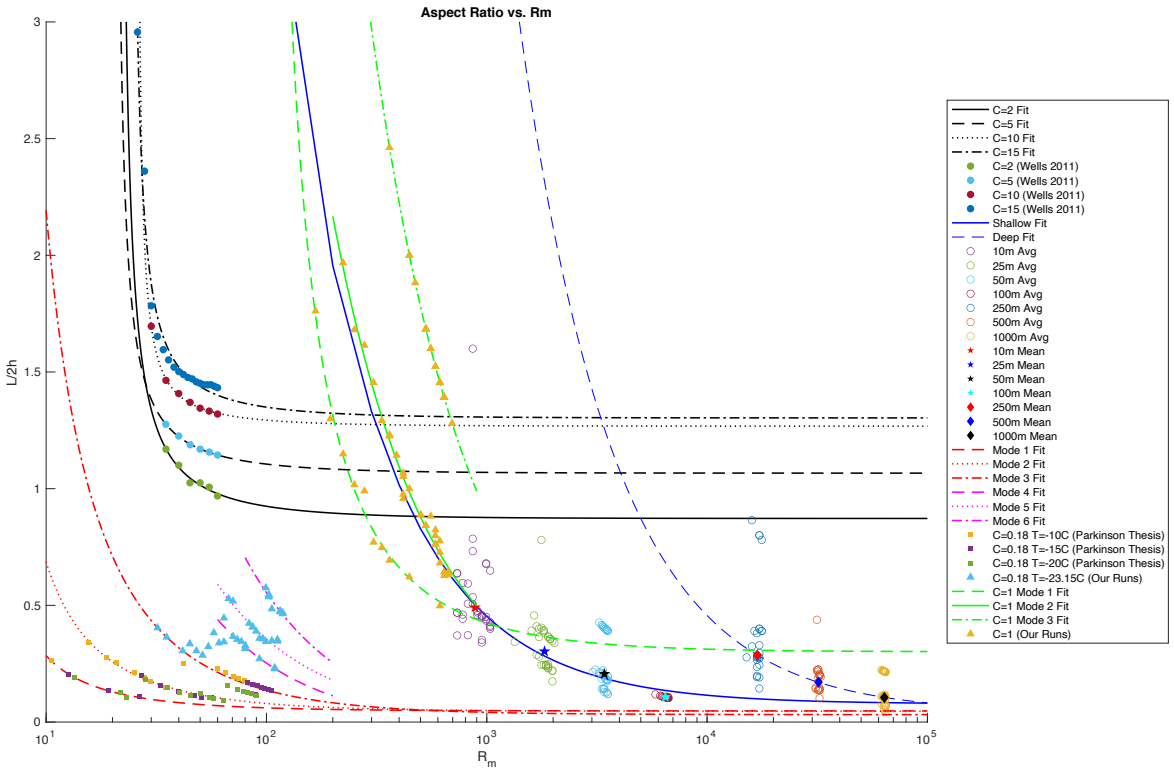

Figure S6. Brine channel aspect ratio as a function of mush Rayleigh number. Solid circles are results from Wells et al. (2011) and black curves are inverse fits to this data. Solid squares are results from Parkinson (2019) (Chapter 5.1.5) and red curves are inverse fits to this data. Open circles and solid stars/diamonds are simulation results and mean values for Europan environments runs, respectively, and blue curves are inverse fits to this data. Blue and yellow solid triangles correspond to our sea ice and $\mathcal{C} = 1$ simiulations, respectively, and the pink and green curves are their associated inverse fits. As the mush Rayleigh number increases brine channel aspect ratios approach a steady state value primarily governed by the concentration ratio, in agreement with the results of (Wells et al., 2011). 'Modes', as listed in the figure legend, are associated with mushy layer convective modes within simulation domains. These quasi-steady states are a common feature of convection in a confined porous media (Karani & Huber, 2017) and are amplified by the finite resolution of simulations.